Computers and Electronics in Agriculture 119 (2015) 133–141

Contents lists available at ScienceDirect

Computers and Electronics in Agriculture

journal homepage: www.elsevier.com/locate/compag

Original papers

Grain bin monitoring via electromagnetic imaging

Mohammad Asefi [a], Ian Jeffrey [a], Joe LoVetri [a,*], Colin Gilmore [b], Paul Card [b], Jitendra Paliwal [c]

[a] Department of Electrical and Computer Engineering, Room E2-390 EITC Building, University of Manitoba, 75 Chancellor's Circle, Winnipeg, MB R3T 5V6, Canada
[b] 151 Research Inc, Canada
[c] Department of Biosystems Engineering, Room E2-376 EITC Building, University of Manitoba, 75 Chancellor's Circle, Winnipeg, MB R3T 2N2, Canada

ARTICLE INFO

Article history:
Received 27 July 2015
Received in revised form 22 October 2015
Accepted 23 October 2015

Keywords:
Grain bin imaging
Microwave imaging
Electromagnetic imaging
Grain bin monitoring
Three-dimensional imaging

ABSTRACT

Stored grain monitoring is an important post-harvest stage of the food production chain. Grains are usually stored in large metal containers referred to as bins or silos. During storage, there is a possibility for grain to spoil and become unusable. Therefore, monitoring of grain bins is essential to detect conditions leading to spoilage within the bin. Most current grain bin monitoring techniques lack sensitivity as they require conditions leading to spoilage to surpass a certain limit before detection is possible, and consequently a large amount of stored grain is lost during monitored storage. This paper presents the advances in developing a novel grain-monitoring technique using electromagnetic imaging, a modality that can provide global, quantitative images of grain properties throughout the bin. Side-mounted antennas illuminate the contents of the bin and a set of receivers measures the electromagnetic energy within the bin at discrete locations. Using these measurements an optimization algorithm attempts to reconstruct the contents of the bin – herein a finite-element contrast source inversion (FEM-CSI) algorithm was used. The result is a global map of the electrical properties of the grain throughout the bin. In this work we first present a synthetic validation of the proposed method for a model of a full scale hopper bin using simulations to produce the electromagnetic field data. Next, a scaled experimental system was used to collect data from grain that contained regions of induced contamination. This data was used to produce images that show the applicability of the method in practice. Results suggest that this technology has potential to provide farmers with a reliable and robust method to remotely monitor stored grain, preserving stored food resources and increasing their revenue.

1. Introduction

The ever-growing world population requires reliable and high-quality resources for food. Grains such as wheat and rice constitute the majority of globally consumed daily food: the total wheat and rice-paddy equivalent produced globally in 2011 were 704.08 and 722.76 million tons, respectively (FAO, 2013). Grains are harvested in large quantities and require safe places for storage, typically large metal containers referred to as bins, or silos, are used. Moreover, current challenges in food production due to scarcity of resources, such as limited land and water, as well as increased weather variability caused by climate change, require *enhanced* post-harvest management. Grains are usually stored dry with the hope that their characteristics will remain unchanged during storage. Harvested grain may be stored for periods of a few weeks to a few years before being used (Maier et al., 2010; Muir, 1998), and a major concern during this period is the possibility of unacceptable deterioration (Maier et al., 2010; Muir, 1998; Metz et al., 2007). Changes in temperature, humidity, moisture content, and external agents such as insects, birds and rodents, can cause spoilage and mold. These factors can cause losses of 3–10% (developed countries) and up to 30% (developing countries) of harvested grain (Muir and White, 2000). To prevent grain contamination, and to extend viability, grain bins should be monitored periodically. This can be performed either *in situ* or *ex situ*. Moisture content and temperature are the most important factors contributing to grain quality. Immunity to different insects and pathogens is also a factor. For instance, insect activities begin at temperatures above 15 °C and mold growth increases at relative humidities over 70% and temperatures between 25 °C and 35 °C (Millls, 1989). Insects and mold in a grain bin can cause small high temperature pockets (known as hot-spots) to form, accelerating deterioration. For example, insect reproduction can result in the creation of pockets of 42 °C, while mold can lead to the production of mycotoxins that can heat up localized regions (Maier et al., 2010; Muir, 1998; Metz et al., 2007). Maintaining uniform temperature and moisture content during storage, as well as early detection of hot-spots so that

* Corresponding author.
E-mail address: Joe.LoVetri@umanitoba.ca (J. LoVetri).

http://dx.doi.org/10.1016/j.compag.2015.10.016
0168-1699/

appropriate action can be taken before major losses occur, are important. Different methods have been developed and applied in grain bin management to monitor grain quality during storage and detect possible contaminations (Maier et al., 2010). The most basic of these techniques is 'human sensory exposure' where a person enters a grain bin and inspects the grain visually by taking samples and/or smelling the ventilated air to determine if mold has formed (Maier et al., 2010; White, 2000). This method can be quite time consuming, ineffective for large bins and erroneous as it lacks exhaustiveness and is prone to human error. Also, due to a number of reported fatalities related to farm workers getting trapped upon entry in filled bins, there has been a call from labor unions to bring in regulation to completely seal off bins from human access.

The most common automatic techniques that are widely used for detecting grain spoilage are temperature and moisture measurement. Depending on the size of a silo, one or more temperature and/or moisture sensor carrying cables are vertically hung in each bin (Fig. 1 (Intellifarms, 2009)). The sensors on each cable are typically separated by 1.2 m or more[1] (White, 2000; Intellifarms, 2009), and the number of cables suspended in a grain bin depends on several factors including: the size of the silo (especially its diameter), the climatic conditions and the stored commodity (Shelton, 1998). One of the main advantages of this system is its real-time temperature and moisture monitoring capability. However, the typical sensor spacing of ≈1.2 m on a given cable results in low spatial resolution. Temperature and humidity sensors are locally sensitive, providing detection limited to a radius of 30–60 cm (White, 2000; Intellifarms, 2009; Mills et al., 1989). Grain is a good thermal insulator and a hot-spot far from the sensor can only be detected when it becomes large enough to be within a sensor's range (Muir, 1998; White, 2000). These cables are also expensive and require reinforcing the ceiling of the grain bin to account for forces exerted on the cables during unloading.

Other automated techniques, such as measuring the CO_2 produced by the living organisms inside the bin, or using acoustic sensors to detect sound generated by insects, have also been reported in literature (Muir, 1998; White, 2000; Mills et al., 1989; Maier et al., 2010; Yan et al., 2006). Such techniques, however, have practical limitations to be used in farm-scale bins.

An alternative, automated technique to detect spoilage and mold within grain bins, is to use electromagnetic imaging (EMI). EMI can be adopted for non-invasive estimation of the electrical properties of an object-of-interest (OI). EMI has been extensively used in medical imaging (Meaney et al., 2007; Abubakar et al., 2002; Semenov and Corfield, 2008), security scanners (Sheen et al., 2001), geophysical surveying (Abubakar and Van den Berg, 2000; Abubakar et al., 2008) and industrial non-destructive testing (Zoughi, 2000). Its objective is to obtain quantitative information (such as physical properties) and qualitative information (such as shape and location) regarding an OI and its internal features (Franchois and Pichot, 1997; Joachimowicz et al., 1991). Applied to grain bins, EMI would produce a global map of the electrical properties of grain throughout the bin. The grain industry already infers moisture content, temperature and bulk density of grain through correlation with grains' electrical properties (Nelson et al., 2000; Yan et al., 2006). EMI offers several advantages over existing methods that include: global sensitivity, the use of low-cost electromagnetic radiation[2] and the ability to provide images without disturbing or interacting with the grain. Another feature

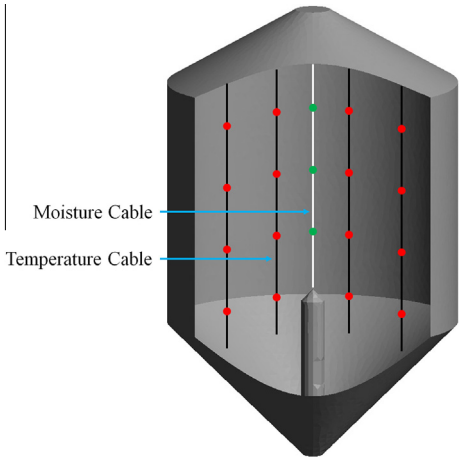

Fig. 1. A typical temperature and moisture grain monitoring system. Cables are suspended from a necessarily reinforced ceiling. Sensors are spaced approximately 1.2 m apart along each cable and are locally sensitive.

that makes EMI a better alternative to current grain bin monitoring techniques is its relatively high spatial resolution compared to existing techniques.[3] Most grain bin monitoring technologies are affected by grain fines and dust. While these particles, over time, can accumulate and coat sensors in the storage bin, the limited thickness of this coating will generally render it invisible to EMI.

We have developed a prototype EMI system capable of monitoring grain bins for early detection of spoilage conditions. The system uses side-mounted antennas to both illuminate the interior of the bin and to collect electromagnetic field measurements. To these measurements we apply an optimization algorithm known as the finite-element contrast source inversion (FEM-CSI) to produce images. In this manuscript, we present synthetic validation of the proposed system and experimental validation from a small-scale prototype.

The paper is organized as follows: a brief description of electromagnetic imaging is given in Section 2; a synthetic validation of the system is outlined in Section 3; a detailed description of the experimental setup, including data calibration and reconstruction results, is presented in Section 4; and finally, the paper concludes, including a brief discussion of our ongoing work, in Section 5.

2. A brief introduction to electromagnetic imaging

EMI is an imaging modality that uses active transmitters and receivers of electromagnetic radiation to obtain quantitative and qualitative images of the complex dielectric profile of an OI. Most EMI systems use antennas as transmitters and/or receivers. Due to the propagation and scattering properties of electromagnetic signals at the lower end of the frequency spectrum (including radio and microwave frequencies), multiple antennas are usually placed such that they surround the OI in order to effectively collect the scattered signal. Each transmitting antenna, in turn, illuminates the OI while the receiving antennas collect the field scattered by the OI. Antennas are connected to an RF multiplexer which switches between the transmitter and receiver pairs. The multiplexer is followed by an electromagnetic (EM) transceiver system. A block diagram of a typical EMI system is provided in Fig. 2. A detailed explanation of the operation of an EMI system is available in (Asefi et al., 2014).

[1] It should be mentioned that in each silo, there is usually one moisture cable and one or more temperature cables.

[2] It is worth mentioning that the cost of the temperature sensor based system for a 45,000 bushel grain bin is approximately $7400 while an EMI system is expected to cost less than $4000 for the same bin size.

[3] Herein, resolution is defined as the smallest spatial step size for which information about the bulk grain is obtained.

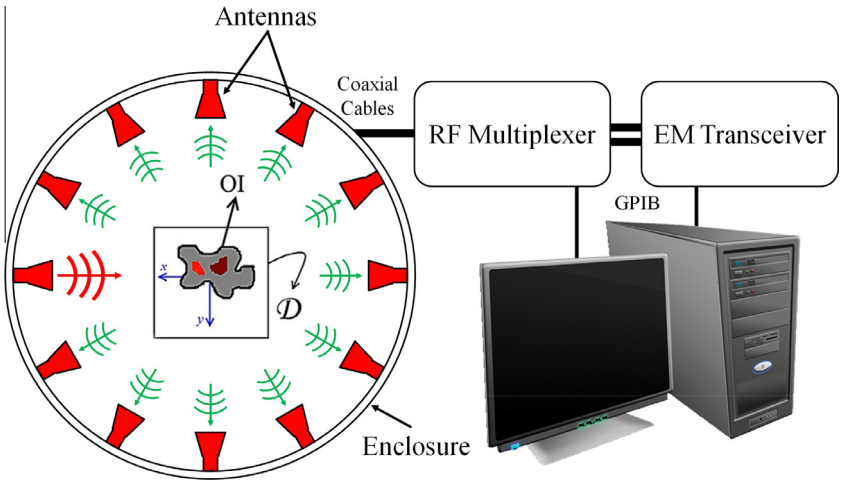

Fig. 2. Block diagram of an EMI system.

The measured data collected by an EMI system are used as the input to an image reconstruction algorithm. These algorithms can be divided into two main categories: those that provide qualitative reconstruction (shape and location) and those that provide quantitative reconstruction (shape, location and OI's electrical properties) (Zoughi, 2000; Zakaria et al., 2010). The imaging system presented herein takes advantage of the features of a *quantitative* image reconstruction algorithm to localize spoilage within the bulk grain and provide a figure of its severity. Applying an imaging algorithm to measurement (or synthetic) data in order to produce images requires solving an electromagnetic inverse problem.

2.1. Electromagnetic inverse problem

Solving an inverse electromagnetic problem involves estimating several attributes of an object-of-interest (OI) using electromagnetic field data collected at several locations surrounding the OI. In this work, the inverse problem is solved using the state-of-the-art contrast source inversion (CSI) algorithm formulated using the finite element method (FEM) (van den Berg and Kleinman, 1997; Zakaria et al., 2010). The resulting algorithm is referred to as FEM-CSI and is an optimization algorithm that estimates the electric properties of an object within a given region so as to minimize a pre-defined objective function. Details on inverse problems can be found in (van den Berg and Kleinman, 1997; Zakaria et al., 2010; Pastorino, 2010). The EMI goal is to reconstruct the relative complex dielectric properties of an OI, denoted by $\epsilon_r(\vec{r})$, at position $\vec{r}$ within an *imaging domain*[4] $\mathcal{D}$ as shown in Fig. 2. The imaging domain is surrounded by transmitters and receivers on a measurement surface[5] (or in a volume).The goal of the FEM-CSI algorithm is to reconstruct the relative permittivity of an OI from measurement data. For matter of convenience, the algorithm reproduces the contrast function $\chi(\vec{r})$ of the OI which is defined as

$$\chi(\vec{r}) = (\epsilon_r(\vec{r}) - \epsilon_b)/\epsilon_b \tag{1}$$

where ϵ_b is the relative permittivity of the background media[6] and $\epsilon_r(\vec{r})$ is the relative permittivity of the OI. The heart of the FEM-CSI algorithm is an FEM forward solver that can produce the fields due to an estimate of the contrast function $\chi(\vec{r})$ (Zakaria et al., 2010; Zakaria and LoVetri, 2012). This forward solver can also be used to predict the behavior of the electromagnetic field within a given region of interest for synthetic data generation. FEM-CSI operates by iteratively updating $\chi(\vec{r})$ until an acceptable error level is obtained between the fields calculated by the forward solver and those of the measurement. This error is quantified by multiple CSI cost functionals including a data misfit cost functional. Consequently, an accurate model of the imaging system is required to correctly reconstruct the OI's properties. A flow chart of the algorithms is presented in Fig. 3. A more detailed explanation of the basic electromagnetic concepts of the algorithm can be found in (Zakaria et al., 2013).

2.2. Grain bin monitoring using EMI

An EMI grain monitoring system is simply an EMI system installed inside a grain bin. Based on the size of typical grain bins (ranging from a few thousand bushels to few hundred thousands of bushels) and the computational resources required for the image reconstruction, it has been found that radio frequencies (RF) are appropriate. The algorithm used herein requires the field scattered by the grain to detect spoilage. The process to obtain this scattered field is as follows:

1. When no spoilage exists in the grain, the bin interior is illuminated and fields are measured. This is referred to as the incident field (E^{inc}). This field is collected shortly after the bin has been filled with grain. Note that for the experimental measurements an electrical/numerical model for the bin contents associated with the incident field measurement is required. An approximate model based on known electrical properties of grain as it comes off the field can be used successfully as shown in Section 4.4.
2. Another field measurement is taken during storage. This measurement is referred to as the total field (E^{tot}).
3. The difference between E^{tot} and E^{inc} is referred to as the scattered field (E^{sct}). If mold or a hot spot have developed, E^{sct} will be non-zero and contain information about the spoilage. This field is used as the input to the image reconstruction algorithm. If E^{sct} is zero, it means that the condition of the grain has not changed.
4. Steps 2 and 3 are repeated periodically during storage. Images are produced for a given time snapshot using E^{sct} associated with that time.

[4] In grain bin monitoring this domain generally extends to the boundaries of the imaging system (*i.e.* the metallic walls of the bin), although it can be selected to be a smaller domain.

[5] Surrounding $\mathcal{D}$ with transmitters/receivers is typical in applications where access to $\mathcal{D}$ is prohibited (*e.g.* medical imaging). For grain bin imaging, transmitters and receivers may exist in $\mathcal{D}$.

[6] The background media can be either homogeneous or inhomogeneous. Herein, the background media is assumed to be homogeneous with a value equal to the permittivity of dry grain.

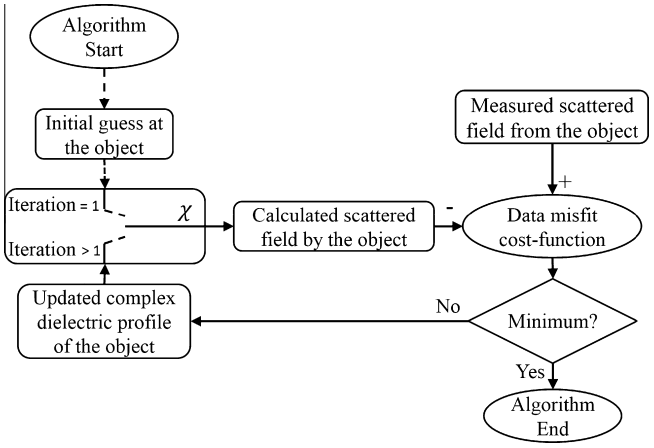

Fig. 3. EMI algorithm flow chart. This flowchart illustrates the process of guessing the electrical properties of an OI using an iterative method.

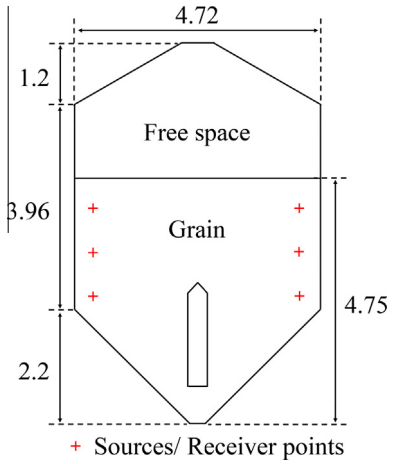

Fig. 4. Hopper style grain bin layout (dimensions are all in meters) modeled for synthetic analysis.

Installing an EMI system inside of a grain bin is a large physical undertaking. Therefore, prior to full-scale experimental deployment, which will be the focus of future work, the feasibility of this technique was numerically examined and a small scale experimental setup was prepared and tested.

3. Synthetic analysis

The software used for synthetic analysis consists of algorithms that solve two problems: an electromagnetic forward problem and an inverse problem. In this part of the study, an assessment was performed to monitor the variation in electromagnetic signals due to the change in grains' electrical properties. This assessment involved running a number of simulations representing scenarios where the electrical properties change due to the presence of moisture, insect infestation, or mold. These forward problems were solved using the FEM forward solver that is part of the FEM-CSI software (Zakaria et al., 2010).

To simulate a full scale grain bin, a 60 tonnes hopper style grain bin at the Canadian Wheat Board Centre for Stored Grain Research (CWBCSGR) at the University of Manitoba, was modeled. The dimensions of the bin are shown in Fig. 4.

To represent grain inside the bin, a medium with relative dielectric permittivity of $2.56 - j0.16$ was used to simulate hard red winter wheat.[7] This permittivity represents a moisture level of approximately 5% (in wet basis) and was measured for 70–100 MHz using a coaxial permittivity measurement device developed at the Electromagnetic Imaging Laboratory (EIL) at the University of Manitoba that is briefly described in Section 4.1. The grain bin walls and the aeration chamber are metallic, and are modeled as perfect electrically conductive (PEC) boundaries. To simulate grain spoilage, a cylindrical target (with a radius of $r = 25$ cm, and a height of $h = 50$ cm) representing spoilage with $\epsilon_r = 4 - j0.66$[8] (corresponding to a moisture level of approximately 18%) was embedded within the grain. The location and size of the target inside the grain bin is illustrated in Fig. 5(a) and (b). It is worth noting that the largest dimension of the target was less than $\lambda/8$ where λ is the RF wavelength in air which is inversely proportional to the RF frequency.

Inside the bin were three layers of 8 equally spaced transmitters. The transmitters were all located within the grain and, for each layer, were distributed on the circumference of a circle with a radius of 1.65 m. The layers were separated by 0.92 m. Transmitters were modeled as electric dipoles polarized along the radius of the chamber ($-\rho$ direction in cylindrical coordinates). Each transmitter, in turn, independently illuminated the bin contents with radio waves at 70 and 90 MHz.[9] The scattered fields were collected at 24 receiver points collocated at the transmitters. 8% white noise was added to the data and different discretizations of the FEM model were used for first generating synthetic data and subsequently performing inversion.[10]

The operational frequency of the proposed system was selected to be within the 65–120 MHz frequency bands that is allocated for Aeronautical radionavigation, fixed mobile and broadcasting (TV and Radio). Since the EMI system is located inside a metallic chamber (shield), there should be almost no interference caused by this system. This frequency range has a wavelength of 3–4 m. Using proper data collection and a well constructed imaging algorithm, resolutions of up to 1/30 of a wavelength can be obtained (Gilmore et al., 2010b). This implies that this system is theoretically capable of 10 cm resolution which is superior to all existing grain monitoring methods.

The FEM-CSI[11] algorithm was used to solve the inverse problem using the synthetic data. The results using the ρ-component of the simulated fields for 70 and 92 MHz are shown in Fig. 6. It is worth mentioning that the inversion mesh for this reconstruction consisted of 212,519 Tetrahedra (corresponding to a mesh with the smallest discritizations of $\lambda/12$ at 92 MHz) and the inversion process took approximately 5 h for 500 iterations. Table 1 provides information on the inversion time required to run 10 iterations for different inversion meshes for the grain bin of Fig. 4. For all measurements, FEM-CSI was run on 16 cores of a 32 core desktop computer with two *Intel*® Xeon(R) CPU (E5-2698 v3 @ 2.30 GHz × 16) and 128.5 GB of DDR4 RAM with a clock speed of 2133 MHz. Note that for a given bin size, higher inversion frequencies require a denser inversion mesh and consequently more computational resources.

In these simulations knowledge of the dry grain distribution (prior to spoilage) was exploited as prior information using a technique referred to as an inhomogeneous background (Zakaria et al., 2010). Also, the imaging domain shown in these images includes

[7] Hard red winter wheat was used in this study as it was available at CWBCSGR for the prototype test phase of this research.

[8] Spoiled grain has higher water content and consequently higher dielectric permittivity compared to the uncontaminated grain. The value used here is to simulated a spot of higher permittivity and conductivity.

[9] These radio frequencies provide a balance between image reconstruction capabilities and computational cost.

[10] This is to avoid what is known as an inverse crime (Zakaria and LoVetri, 2012).

[11] The FEM-CSI algorithm used herein includes a multiplicatively balanced regularizer (MR) to enhance the image reconstruction.

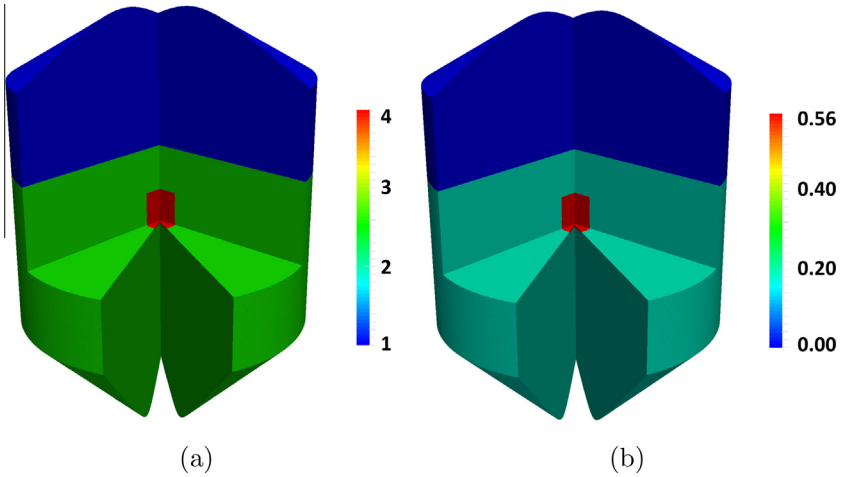

Fig. 5. The real (a) and imaginary (b) parts of the dielectric permittivity distribution used to produce the synthetic data. The dark blue region represents air while the shades of green represent grain and red represents spoilage. (For interpretation of the references to colour in this figure legend, the reader is referred to the web version of this article.)

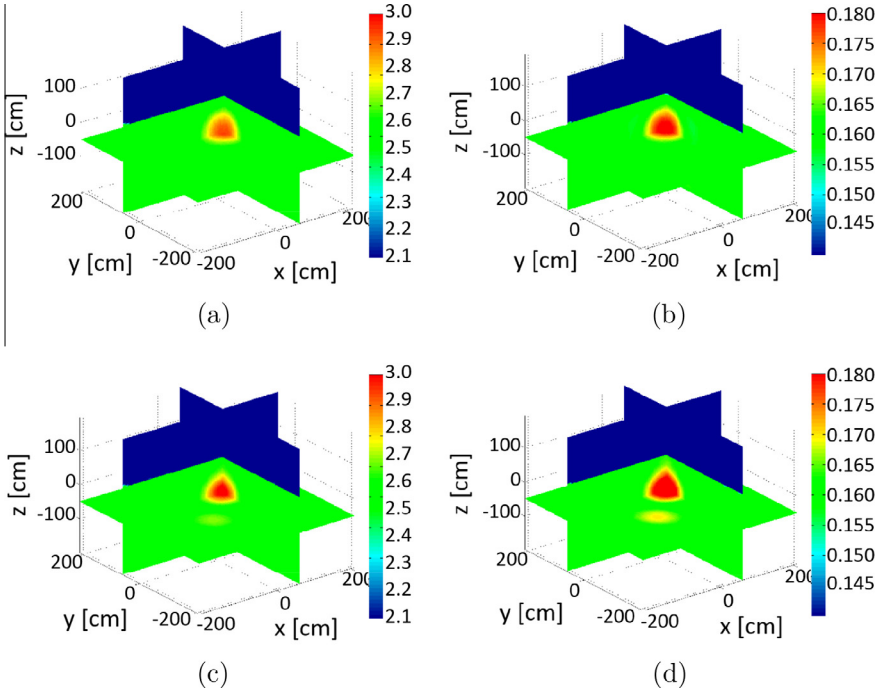

Fig. 6. Real and imaginary parts of the reconstructed dielectric map of the grain for cylindrical spoilage with $r = 25$ cm and $h = 50$ cm at (a and b) 70 MHz and (c and d) 92 MHz for synthetically generated data.

Table 1
Required resources for 10 iteration inversion of $\lambda/10$ discritized meshes on 16 cores.

Frequency (MHz)	Number of tetrahedra	Time per iteration (s)	Inversion time hh:mm:ss	Total memory required (MB)
100	135,314	17.9	00:03:58	11,842
120	262,906	39.8	00:09:47	22,267
150	407,172	72.5	00:18:54	36,382
180	617,924	140	00:37:43	58,105
200	910,690	299	01:21:32	90,509

only limited cross-sections of the grain bin (as opposed to Fig. 5(a) and (b) which shows most of the bin).

In both cases, spoiled grain was reconstructed at the correct location. The value of the $\epsilon_r(\vec{r})$ was not accurately reconstructed (*i.e.* it was smaller than $\epsilon_r = 4 - j0.66$). This is due to the small size of the targets in comparison to the wavelength of the imaging frequency. However, in any synthetic analysis conducted by the authors, it was observed that any change in the dielectric properties of the synthetically generated data is consistent with that of the reconstructed image (*i.e.* if ϵ_r of the spoilage is reduced in the synthetic data, the reconstructed image will have a lower ϵ_r). It was found that moisture levels as low as 8% were still detectable. In a second synthetic experiment, the size of the spoilage was reduced and it was successfully detected as shown in Fig. 7. The largest dimension of the spoilage in this case was smaller than $\lambda/14$.

From the results, it was observed that reducing the size of the spoilage does not reduce the size of the real part of the reconstructed spoiled region, but does reduce the value of ϵ_r. This is

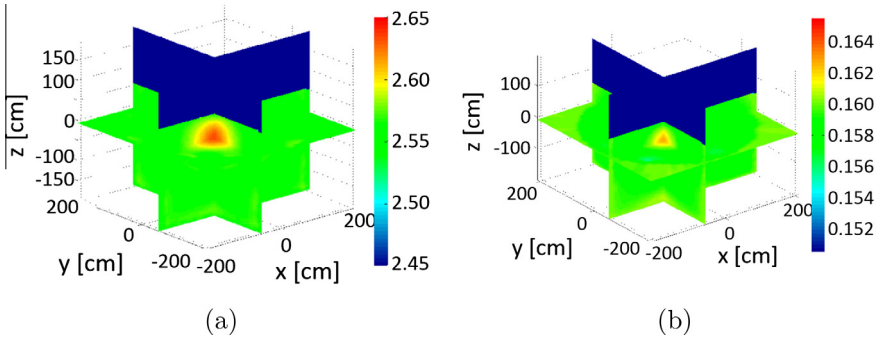

Fig. 7. (a) Real and (b) imaginary parts of the reconstructed dielectric map for cylindrical spoilage with $r = 15$ cm and $h = 30$ cm at 70 MHz for synthetically generated data.

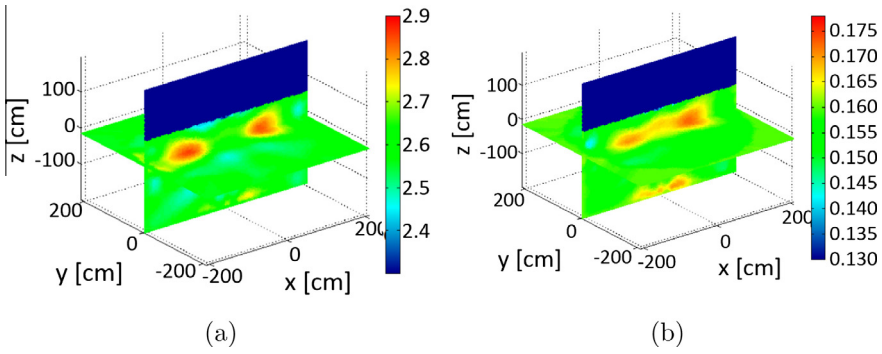

Fig. 8. (a) Real and (b) imaginary parts of the reconstructed dielectric map for multiple spoilage targets at 70 MHz for synthetically generated data.

not surprising given the small target size relative to the wavelength, and is promising as detection is still possible. A reduction in size of the spoiled region is more clear in the imaginary part of the permittivity.

To further investigate the capabilities of the proposed method, a set of synthetically generated data for two contaminated regions inside the bin was generated. The reconstruction results for this case are shown in Fig. 8. The results show separation between the two regions, however, the permittivity of contaminations is still under-estimated.

4. Laboratory-scale experimental system

For the second phase of this feasibility study a laboratory-scale metallic cylindrical chamber, with $r = 15$ cm and $h = 30$ cm, was constructed. This scaled experimental system consists of 24 monopole antennas each 5 cm long, distributed in three layers inside the chamber. The antennas were polarized along the radius of the enclosure ($-\rho$) and were connected to a 24-to-2 RF multiplexer/switch that was followed by a vector network analyzer (VNA) analogous to that shown in Fig. 2. The RF switch enabled each antenna to either deliver the RF energy to the imaging chamber or to collect the RF energy from the other antennas. The VNA was used to generate the RF signals for illuminating the grain and for receiving fields.

4.1. Grain permittivity measurement device

In order to accurately measure the dielectric properties of the grain used in the experiments, a dielectric measurement device was required. Since the imaging technology measures bulk permittivity of grain (on the order of cm), and the stored grain consists of areas of both grain and air (on the order of mm), the bulk measurement of permittivity (as opposed to measuring the permittivity of individual grains) was required. Consequently, a coaxial permittivity measurement device capable of measuring the bulk permittivity of grain was selected and constructed (Yaw, 2012). The permittivity measurement device built for these experiments was made of a coaxial transmission line section and two BNC connectors. The transmission line was made up of five different coaxial sections as illustrated in Fig. 9(a). The first section of this coaxial line (from both sides) was used to connect the transmission line to the measurement equipment through BNC connectors (one end of the BNC connectors gets connected to the center connector of the coaxial line). The outer flat part of the connector for this section was used as a cap for the coaxial sample holder containing grain samples within the device. The second section, which includes an ultra high molecular weight (UHMW) dielectric material, was used as a mechanical support to hold the center connector in place. The middle part of this coaxial line is a 50 Ω air field chamber which can be filled with the material whose dielectric characteristics are to be determined. The cut-off frequency of this sample holder is 1.962 GHz. The device was built using aluminum for both the center and the outer conductor. A snapshot of the fabricated permittivity measurement device is shown in Fig. 9(b).

This device was used to measure electrical properties of hard red winter wheat at different moisture levels over the frequency range of 30–200 MHz. The permittivity of this grain was assumed to be constant within this frequency range based on the results presented in (Nelson and Stetson, 1976), and measurement results are presented in Table 2.

4.2. Data collection system

Each antenna that was used in the scheme shown in Fig. 2 could operate in either transmit or collect mode. The former mode 'delivered' the energy from the RF source to the chamber. The latter mode 'collected' the energy at the location of the antenna. The

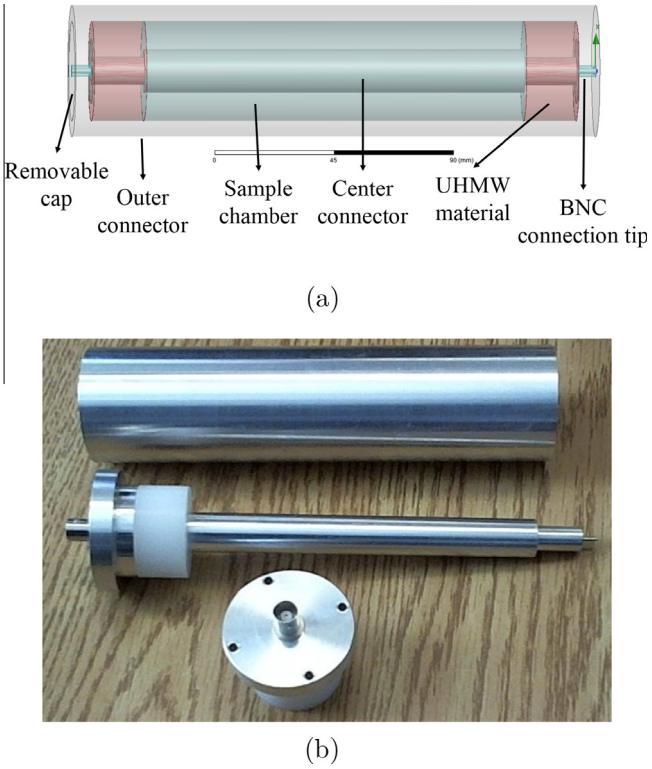

Fig. 9. An illustration of the coaxial dielectric measurement device (a) and its disassembled sections (b).

Table 2
Electrical properties of hard red winter wheat for 30–200 MHz frequency band.

Moisture content (%)	ϵ'	ϵ''
9.3	3.16	0.36
11.7	3.34	0.44
13.7	3.8	0.467
17.5	4.06	0.56
18.2	4.6	0.6
24.2	4.96	0.64

transmit/collect antennas were selected through the RF switch. After selecting an antenna as the transmitter, it illuminated the interior of the bin and the remaining antennas received the fields. The field received by the collector antennas was measured by the VNA as an S-parameter, and is related to the field at the location of the collector antenna. The data acquisition system used for data collection is shown in Fig. 10. Two sets of measurements ware required (as explained in Section 2.2): a measurement before any contamination exists in the chamber, denoted as the $\vec{E}^{\text{inc}}$, and a measurement with the presence of an induced contamination inside the chamber that is referred to as the total field ($\vec{E}^{\text{tot}}$).

4.3. Calibration

The forward solver in the FEM-CSI image reconstruction algorithm does not fully model the measurement system and antennas. It uses antenna models (ideal dipoles) and calibration is required to account for the difference between the true EMI system antennas (and other objects in the system that were not modeled) and the simplified forward solver model. The task of calibrating an imaging system is highly dependent on the system configuration. Several calibration techniques have been reported in the literature,

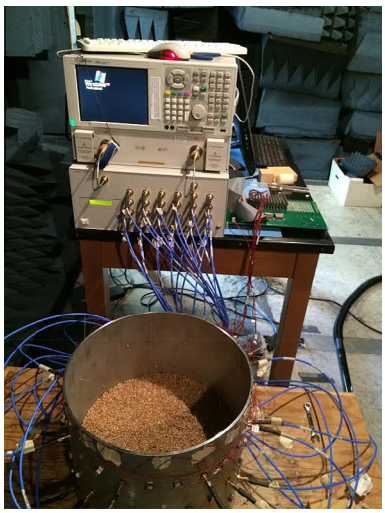

Fig. 10. The data acquisition system including the VNA, RF switch and the metallic enclosure filled with grain.

e.g. using the incident-field, or using the scattered-field of a known reference object (Gilmore et al., 2010a). It was found that an inhomogeneous-background incident-field calibration is appropriate. This calibration technique uses Eq. (2) to compute calibrated measured fields ($E^{\text{sct, cal}}$).

$$E^{\text{sct, cal}} = \left(E^{\text{tot|OI}} - E^{\text{inc}}\right)\frac{\widetilde{E}^{\text{inc}}}{E^{\text{inc}}} \tag{2}$$

Here, (E^{inc}) is the incident field *measured* in the filled chamber with known properties, $E^{\text{tot|OI}}$ is the total field *measured* when the induced spoilage exists in the chamber, and $\widetilde{E}^{\text{inc}}$ is the incident field *simulated* for the known inhomogeneous background (*dry grain's permittivity*).

4.4. Experimental laboratory-scale EMI system results

Two sets of data were collected for cases where a target was buried under the grain at different locations inside the metallic enclosure of Fig. 10. The target is illustrated in Fig. 11. The FEM-CSI algorithm was used to reconstruct the grains' electrical properties using the calibrated data. As the metallic enclosure was small compared to a full size grain bin, the frequency for data collection and image reconstruction was increased to 1.1 GHz. Note that the size of the target in this setup was approximately $\lambda/7$. Fig. 12(a)–(d) shows the real and imaginary parts of the reconstructed dielectric map when the target was buried at two different locations.

Fig. 11. Spoiled grain used as the target. Hard red winter wheat with a 20% moisture level was placed inside a plastic container over 1 month to obtain uniformly spoiled grain.

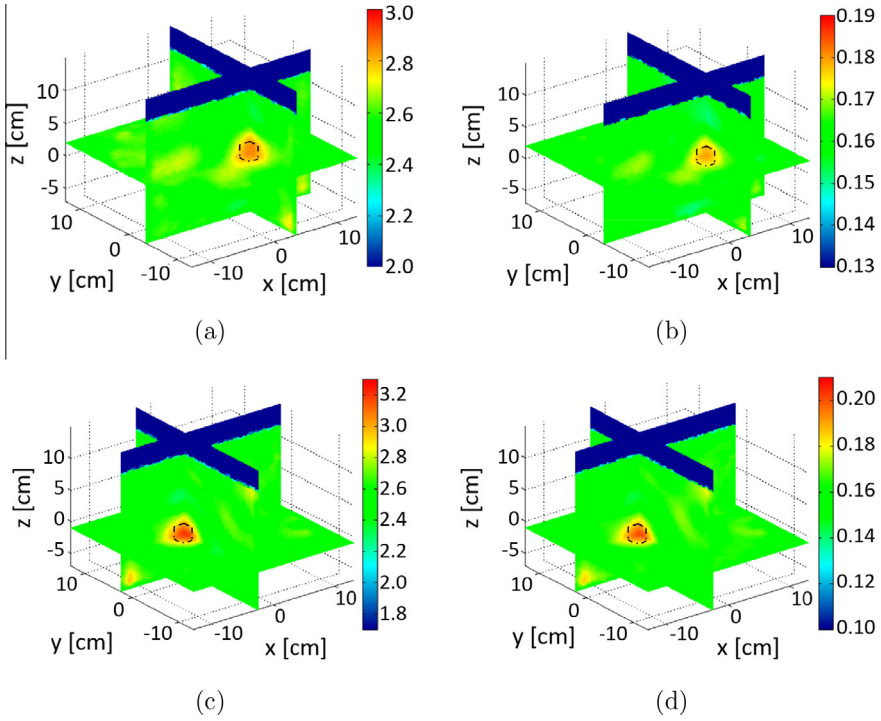

Fig. 12. Real and imaginary parts of the reconstructed dielectric map of the grain at 1.1 GHz at multiple locations for experimentally measured data. Dashed lines mark the actual size and location of the target.

These results show successful detection of the contamination at their correct locations in both cases. However, due to the very small size of the contamination (compared to wavelength), the reconstructed size of the target is not accurate. To ensure that the reconstructed dielectric profile is that of the spoiled grain rather than the container holding it, the container was filled with uncontaminated grain and buried at the same locations. The measured electric field was then compared to that of the case when no container was placed inside the chamber (E^{inc}). As expected, no changes were observed since the thickness of the container (0.8 mm) compared to the wavelength at the measurement frequency (272.7 mm) is negligible.

5. Conclusion

Successful detection of grain spoilage using EMI has been presented for both synthetic and experimental data sets. The installation and analysis of an EMI system inside a hopper style grain bin at the CWBCSGR at the University of Manitoba is ongoing. Future work will evaluate EMI grain bin monitoring at scale during grain storage. Studies show that the dielectric properties of materials are also dependent on their temperature level (Ryynänen, 1995). Use of the proposed grain monitoring technique for detection of grain's moisture content and temperature variations during storage will be investigated. Long-term, full-scale, grain bin monitoring using this modality to study the effects of instrument drift and uniform non-decay changes in the grain will be important parts of future research.

Acknowledgments

The authors would like to thank Dr. Amer Zakaria for the access to his FEM-CSI algorithm, Dr. Majid Ostadrahimi for his technical advise and Dr. Fuji Jian for his help at the CWBCGSR facility. The authors would also like to thank Mitacs – Canada for their financial support.

References

Abubakar, A., Van den Berg, P.M., 2000. Non-linear three-dimensional inversion of cross-well electrical measurements. Geophys. Prospect. 48, 109–134.
Abubakar, A., van den Berg, P.M., Mallorqui, J.J., 2002. Imaging of biomedical data using a multiplicative regularized contrast source inversion method. IEEE Trans. Microwave Theory Tech. 50, 1761–1777.
Abubakar, A., Habashy, T.M., Druskin, V.L., Knizhnerman, L., Alumbaugh, D., 2008. 2.5D forward and inverse modeling for interpreting low-frequency electromagnetic measurements. Geophysics 73, F165–F177.
Asefi, M., OstadRahimi, M., Zakaria, A., LoVetri, J., 2014. A 3-d dual-polarized near-field microwave imaging system. IEEE Trans. Microw. Theory Tech.
van den Berg, P.M., Kleinman, R.E., 1997. A contrast source inversion method. Inverse Prob. 13, 1607.
FAO, 2013. Production. <http://faostat3.fao.org/home/index.html#HOME> July 19, 2013.
Franchois, A., Pichot, C., 1997. Microwave imaging-complex permittivity reconstruction with a Levenberg–Marquardt method. IEEE Trans. Antenn. Propag. 45, 203–215.
Gilmore, C., Mojabi, P., Zakaria, A., Ostadrahimi, M., Kaye, C., Noghanian, S., Shafai, L., Pistorius, S., LoVetri, J., 2010a. A wideband microwave tomography system with a novel frequency selection procedure. IEEE Trans. Biomed. Eng. 57, 894–904.
Gilmore, C., Mojabi, P., Zakaria, A., Pistorius, S., LoVetri, J., 2010b. On super-resolution with an experimental microwave tomography system. IEEE Antenn. Wireless Propag. Lett. 9, 393–396.
Intellifarms, 2009. Moisture cable. <https://intellifarms.com/solutions/binmanager/Moisture_Cable.html.aug> (23, 2012).
Joachimowicz, N., Pichot, C., Hugonin, J.P., 1991. Inverse scattering: an iterative numerical method for electromagnetic imaging. IEEE Trans. Antenn. Propag. 39, 1742–1753.
Maier, D., Channaiah, L., Martinez-Kawas, A., Lawrence, J., Chaves, E., Coradi, P., Fromme, G., 2010. Monitoring carbon dioxide concentration for early detection of spoilage in stored grain. Julius-Kühn-Archiv, S-505.
Meaney, P.M., Fanning, M.W., Raynolds, T., Fox., C.J., Fang, Q., Kogel, C.A., Poplack, S. P., Paulsen, K.D., 2007. Initial clinical experience with microwave breast imaging in women with normal mammography. Acad Radiol.
Metz, N., Group, C., Association, S.E.P.W., et al., 2007. The WA guide to high moisture harvest management, grain storage and handling. CBH Group.
Millls, J., 1989. Spoilage and Heating of Stored Agricultural Products. <https://www.grainscanada.gc.ca/storage-entrepose/jmills/shsap-depae-eng.htm>.
Mills, J.T., et al., 1989. Spoilage and heating of stored agricultural products. Prevention, detection and control. Minister of Supply and Services.
Muir, W., 1998. Grain Preservation Biosystems. University of Manitoba, Winnipeg.
Muir, W., White, N., 2000. Microorganisms in stored grain. Manitoba: Grain Preservation Biosyst., 1–17
Nelson, S., Stetson, L., 1976. Frequency and moisture dependence of the dielectric properties of hard red winter wheat. J. Agric. Eng. Res. 21, 181–192.

Nelson, S.O., Kraszewski, A.W., Trabelsi, S., Lawrence, K.C., 2000. Using cereal grain permittivity for sensing moisture content. IEEE Trans. Instrum. Meas. 49, 470–475.

Pastorino, M., 2010. Microwave Imaging, vol. 208. John Wiley & Sons.

Ryynänen, S., 1995. The electromagnetic properties of food materials: a review of the basic principles. J. Food Eng. 26, 409–429.

Semenov, S.Y., Corfield, D.R., 2008. Microwave tomography for brain imaging: feasibility assessment for stroke detection. Int. J. Antenn. Propag. 2008, 8.

Sheen, D., McMakin, D., Hall, T., 2001. Three-dimensional millimeter-wave imaging for concealed weapon detection. IEEE Trans. Microw. Theory Tech. 49, 1581–1592.

Shelton, D.P., 1998. Management – The Key to Maintaining Stored Grain Quality. <http://lancaster.unl.edu/ag/crops/inservice/manage-i98.html> July 22, 2014.

White, N., 2000. Protection of Farm-Stored Grains, Oilseeds, and Pulses from Insects, Mites and Molds. Cereal Research Centre, Agriculture and Agri-Food Canada.

Yan, H., Chen, G., Li, Z., Dong, Y., 2006. Preliminary research on measurement of stored-grain temperature by acoustic method. In: The Sixth World Congress on Intelligent Control and Automation, 2006. WCICA 2006. IEEE, pp. 5245–5249.

Yaw, K.C., 2012. Measurement of Dielectric Material Properties. Technical Report. Rohde & Schwarz.

Zakaria, A., Gilmore, C., LoVetri, J., 2010. Finite-element contrast source inversion method for microwave imaging. Inverse Probl. 26, 115010.

Zakaria, A., Jeffrey, I., LoVetri, J., 2013. Full-vectorial parallel finite-element contrast source inversion method. Prog. Electrom. Res. 142, 463–483.

Zakaria, A., LoVetri, J., 2012. The finite-element method contrast source inversion algorithm for 2d transverse electric vectorial problems. IEEE Tran. Antenn. Propag. 60, 4757–4765.

Zoughi, R., 2000. Microwave Non-Destructive Testing and Evaluation. Kluwer Academic Publishers.